Three-dimensional in vivo near-infrared photoacoustic tomography of whole small animal head

Kwang Hyun Song, George Stoica, Lihong V. Wang

Kwang Hyun Song, George Stoica, Lihong V. Wang, "Three-dimensional in vivo near-infrared photoacoustic tomography of whole small animal head," Proc. SPIE 6086, Photons Plus Ultrasound: Imaging and Sensing 2006: The Seventh Conference on Biomedical Thermoacoustics, Optoacoustics, and Acousto-optics, 60860Q (6 March 2006); doi: 10.1117/12.646681

SPIE.

Event: SPIE BiOS, 2006, San Jose, California, United States

Three-dimensional *In Vivo* Near-infrared Photoacoustic Tomography of Whole Small Animal Head

Kwang Hyun Song[1], George Stoica[2], Lihong V. Wang[1*]
[1]Optical Imaging Laboratory, Department of Biomedical Engineering, Texas A&M University
[2]Department of Pathobiology, Texas A&M University

ABSTRACT

A three-dimensional *in vivo* near-infrared photoacoustic tomography imaging system was newly designed and built to visualize the structure of a whole small animal head. For high sensitivity, a single flat 2.25MHz low frequency transducer, whose active element size is 6mm, was employed. To increase the penetration depth of light, a wavelength of 804nm in the NIR range, which matches the oxy- and deoxy-hemoglobin isosbestic point, was chosen. To avoid strong photoacoustic signal generation from the skin surface, we applied dark field illumination. To illuminate efficiently, we split the laser light into two beams, which were delivered to an animal by two mirrors and were finally homogenized by two ground glasses. To complete the dark field illumination, the transducer was located in the middle of two light sources. Two key devices for the *in vivo* imaging were rotating devices and animal holders. The rotating devices were composed of two parts, located at the top and bottom, which rotated at the same angular speed. The holders were composed of a head holder and a body holder. Both holders fixed the animal firmly to reduce motion artifacts. This system achieved radial resolution of up to 260μm. We accomplished successful *in vivo* imaging of arterial and venous vessels deeply, as well as superficially, with the animal head of up to 1.7cm diameter. The technique forms a basis for functional imaging, such as measurement of the oxygen consumption ratio in the brain, which is a vital parameter in a brain disease research.

Keywords: three-dimensional, *in vivo*, photoacoustic, rotating devices, mouse holder

1. INTRODUCTION

Photoacoustic tomography (PAT) holds great promise as an optical imaging modality. The most obvious advantage of this modality is that it is non-ionizing, and highly sensitive to optical absorption in biological tissues, especially blood vessels[1], and excellent for deeper imaging.[2-5] PAT combines the advantages of both the optical and ultrasonic imaging modalities. The optical imaging modality has high optical contrast but poor resolution, which results from a loss of information due to strong light scattering at depths of more than one transport mean free path. On the other hand, ultrasonic imaging has high spatial resolution but poor contrast. PAT, however, provides both high ultrasonic spatial resolution and good optical contrast.[2-5]

The photoacoustic effect was discovered in the nineteenth century and Alexander Graham Bell was the first to describe the photoacoustic effect in the field of photophone, but the technology did not yet exist to take advantage of it for imaging. Many years later, Hoelen,*et al* demonstrated three-dimensional blood vessel images of capillaries filled with blood inside chicken tissue. In this study, he achieved up to 10μm as the resolution of his system.[6] Wang, *et al* also successfully applied this technique, from the axial view, to the *in vivo* imaging of blood vessels on the cortex of the brains of small animals.[5,7] He also acquired *in situ* three-dimensional mouse brain imaging from the axial view with satisfactory resolution. However, the deeper images showed structures much less clearly than the images from near the cortex surface.[8] Kruger, *et al* also conducted *in situ* three-dimensional whole head imaging of a nude mouse from the coronal view using an ultrasonic transducer array.[9] In his study, superficial vessels, like the jugular vein, were imaged with good spatial resolution and contrast; though again, deeply located vessels were not clearly imaged.

Therefore, in this study, our main objective was to accomplish *in vivo* three-dimensional whole head imaging. For this purpose, we recently designed an *in vivo* whole head imaging system using photoacoustic tomography (PAT). We

* e-mail: lwang@tamu.edu, tel: +1-979-847-9040

Photons Plus Ultrasound: Imaging and Sensing 2006: The 7th Conference on Biomedical Thermoacoustics, Optoacoustics, and Acousto-optics, edited by A. A. Oraevsky, et. al
Proc. of SPIE Vol. 6086, 60860Q (2006) • 1605-7422/06/$15 • doi: 10.1117/12.646681

successfully imaged the deep arterial vessels as well as the superficial venous vessels with good spatial resolution and high contrast. This imaging system was also able to provide depth information about specific structures by using the coronal view, rather than the axial view, which has been widely used in the literature.[4,5,7,8]

2. SYSTEM DESIGN AND METHOD

For *in vivo* whole head imaging, we designed a new imaging system that is described below. Figure 1 shows a schematic diagram of the system. We used a Q-switch Nd:YAG laser (LS-2137/2, LOTIS TII) pumped tunable Ti:Sa laser (LT-2211A, LOTIS TII) as the excitation source to provide 15-ns laser pulses with a 10Hz pulse repetition rate. To illuminate efficiently, the laser light was divided into two beams by a beam splitter (BS1-784-50, CVI Laser), delivered to the animal by two mirrors, and finally homogenized by two ground glasses. The light sources were positioned at a 135 degree angle which was determined by a Monte Carlo simulation. For the deeply penetrating light needed to conduct the whole head imaging, we chose an 804nm wavelength in the NIR range. This wavelength is also the isosbestic point for both oxy- and deoxy-hemoglobin.

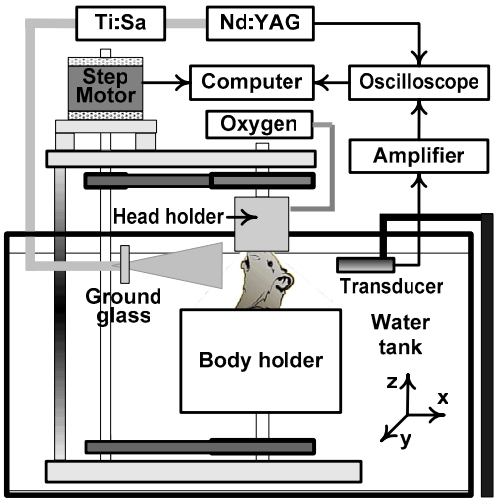

Figure.1: Schematic diagram of the *in vivo* whole head imaging system using photoacoustic tomography. The signals received by an ultrasonic transducer are digitized by oscilloscope and collected by computer. All mechanical movements are controlled by the computer.

We kept the energy of the laser light below 31mJ/cm^2 to satisfy the maximum permissible exposure (MPE) limit for skin at the 804nm wavelength.[10] To avoid strong photoacoustic (PA) signal generation from the surface of the object, we applied the dark field illumination in contrast to bright field illumination.[11] To expand an imaging area for three-dimensional imaging and to enable full body imaging, we chose side illumination instead of top illumination. To avoid direct light illumination on the transducer surface, which causes the generation of undesirable signals, we turned the animal 360 degrees instead of turning the transducer.

High sensitivity was also indispensable for detecting weak PA signals from locations deep within the animal. Therefore, we employed a single flat 2.25MHz low frequency ultrasonic transducer (V323, Panametrics-NDT, Waltham, MA), with a 6mm diameter active element and a 65.6% nominal bandwidth. We made this choice because low frequency ultrasonic signals suffer from less attenuation than higher ones and wide active-element transducers have higher sensitivity than narrow ones. The transducer also provided satisfactory resolution for the imaging. Employing a flat transducer means that an algorithm-modified back projection can be used for reconstruction,[3,12] because a flat transducer, especially low frequency, has wide receiving angle and covers all the imaging plane of the animal head. The modified back projection algorithm is based on two assumptions: the homogeneous light energy and homogeneous acoustic speed distributions on the imaging plane. To form the dark field illumination and to detect the PA signals

efficiently, the transducer was located at the middle of two light sources with a 4cm radius from the center of the imaging plane.

An amplifier (5072PR, Panametrics-NDT) amplified the PA signals received by the transducer, and an oscilloscope (Tektronix TDS 5054) digitized them at a rate of 125MHz. Finally, the computer collected all of the digitized signals and reconstructed the distribution of the optical absorption on the imaging plane.

For the *in vivo* whole head imaging, we designed two new devices: translational stages and animal holders. The translational stages were composed of two parts, a horizontal rotating stage and a vertical linear stage. The horizontal rotating stage had two parts, located at the top (above the head holder) and the bottom (below the body holder), all of which were controlled by the computer to rotate 360 degrees at the same angular speed as the tomography. The vertical linear stage was used for three-dimensional imaging. The holders were composed of the head holder and the body holder. The head holder fixed the head and provided oxygen to the animal while the body holder fixed the animal body and maintained its temperature during the experiment. The body holder was waterproof because the animal and the transducer were immersed in water to couple them with the acoustic waves. We chose 122 steps for a full 2π scan and a 30 times signal average based on the data acquisition time and the SNR.[4,13]

3. EXPERIMENTAL RESULTS

1.1. Phantoms

In order to test the system and to measure its resolution, we imaged 2 human hair fibers and 9 carbon fibers, with diameters of 30μm and 6μm respectively. The turbid medium was composed of 15% porcine gelatin and 0.5% intralipid-20%, whose scattering coefficient was estimated at 2.05[cm^{-1}].[14] The shape of the phantom was cylindrical with a diameter of approximately 2.5cm, imitating the size and shape of a small animal head from the coronal view. Carbon fibers were located at approximately every 1mm and were perpendicular to the imaging plane.

Figure 2A shows a photoacoustic (PA) image of the phantom with a 35mm × 35mm field of view (FOV). Bright spots in figure 2A represent the high optical absorption of the fibers. To quantify the radial and tangential resolutions, we selected carbon fibers. We define the resolution for the radial and tangential direction as the Full Width Half Maximum (FWHM) of the main lobe of the carbon fibers. The FWHM along the radial direction was measured at approximately 260μm, which is almost constant through all carbon fibers and close to the theoretical value described in the reference.[12]

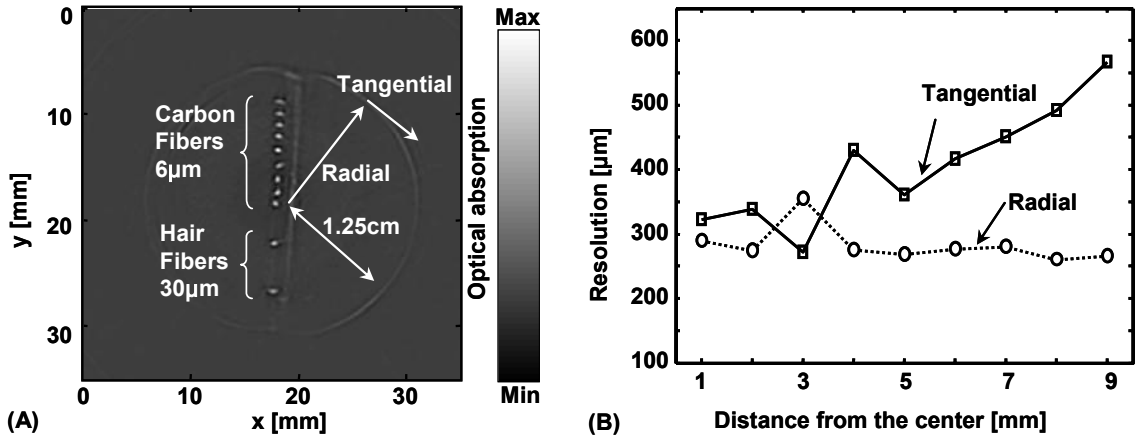

Figure 2A: Photoacoustic image of 9 carbon fibers and two hair fibers in 15% porcine gelatin with 0.5% intralipid-20% (reduced scattering coefficient is 2.05 [cm^{-1}]). The fibers were perpendicular to the imaging plane. [Note: every fiber was not exactly perpendicular to the image plane, so the distortion existed due to the thick slice thickness].

Figure 2B: Radial and tangential resolution of the system. Both are defined as the FWHM of the main lobe of carbon fibers along corresponding directions. The dashed line with circles shows the radial resolution of up to 260μm. The solid line with squares represents the tangential resolution. This resolution is getting worse along x-axis. This explains the aperture effect of the transducer.

Near the center, the shape of the carbon fibers is a circle, but near the outside, it becomes elliptical along the tangential direction. Therefore, we can draw the conclusion that the tangential resolution of the system becomes worse as the imaging point moves farther away from the center of the imaging plane as shown in figure 2B. This is called the aperture effect, and it occurs when the element size of the transducer is larger than the wavelength of the acoustic wave.[4,12] In addition, when a long and narrow object, like the fibers in the figure 2A, is not perpendicular to the imaging plane, the PA image of the object will not show the same shape of the cross section. Also, it will be an oval shape because a flat transducer receives signals from a wide range of volumes. The fourth carbon fiber from the center shows this type of distortion.

1.2. *In vivo* experiment

For the *in vivo* whole head imaging, a nude mouse (Harlan Co.) weighing around 20g was employed. General anesthesia, which was a mixture of hydrochloride (44 mg/kg), xylazine hydrochloride (2.5 mg/kg), acepromazine maleate (0.75 mg/kg), and atropine (0.025 mg/kg), was subcutaneously administered to the nude mouse every hour during the experiment. To reduce light scattering from the hair, the hair on the mouse heads was gently removed using a commercial hair-removal lotion before imaging. During data acquisition, pure oxygen was provided through the head holder. The diameter of the nude mouse head that we imaged was around 1.5cm.

Figure 3A shows the photoacoustic tomography of the nude mouse in a certain imaging plane. The bright spots represent high optical absorption at the 804nm wavelength. At this wavelength, the high optical absorbers are mainly blood vessels, which were marked with arrows and numbers. They were named in the caption of figure 3A. Figure 3B is a photo of a cross section of a nude mouse head which is provided for comparison with the PAT image. The major blood vessels in the figure 3A are well matched with the ones in figure 3B. Deep arterial blood vessels, shown by numbers 1 and 5, are the arterial circle of Willis, which provide oxygen to the brain. Number 9, 10, and 12 are big venous vessels from the jugular vein located superficially.

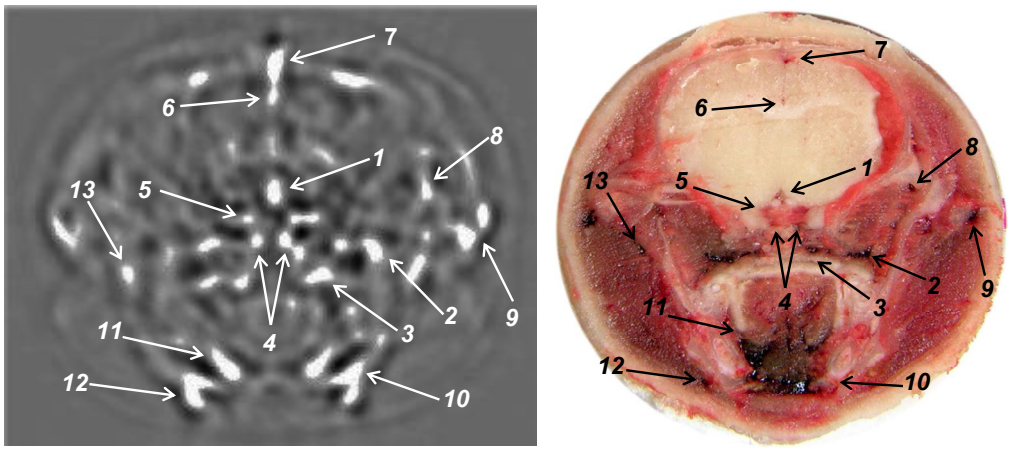

(A) PAT image **(B) Cross section photo of nude mouse**

Figure.3A: PAT image from the coronal view. The field of view is 17mm x 14mm. The predominant blood vessels are marked with arrows and numbers; they were separated by a threshold and superimposed on the structural image. Compensation for optical attenuation was included.
Figure.3B: A histological picture of a cross section of a nude mouse head. 1. Anterior Cerebral Artery; 2. Mandibular Alveolar Artery; 3, 4. Arterial Vessels; 5. Posterior Communication Artery; 6. Internal Cerebral Artery; 7. Median Fissure; 8. Venous Vessel; 9. Facial Vein; 10. Facial Artery; 11. Sublingual Artery; 12. Jugular Vein; 13. Venous Vessel.

To achieve three-dimensional whole head images, we changed the vertical position every 1mm by adjusting the vertical linear stage manually, and then scanned until the whole head was covered. Figure 4 depicts the *in vivo* three-dimensional whole-head images of the nude mouse obtained from the anterior to the posterior parts every 1mm. The

bright spots also represent the high optical absorption and represent the dominant blood vessels. Most of the structures are connected throughout the images due to the head vasculature; some of them are not. The names of the major blood vessels are shown in the caption of figure 3B. Most of the blood vessels that we imaged are tributaries of the common carotid artery and the jugular vein. When we consider functional imaging of the brain, the arterial circle of Willis, as mentioned before, is important for monitoring the brain activity. These vessels are located at the bottom and in the middle of the brain and provide collateral blood flow to the brain. All images were filtered by band-pass filters and were compensated for light attenuation. The blood vessels, which are not perpendicular to the imaging plane, look elliptical as shown in the phantoms experiment because of the undefined slice thickness. Also, the resolution deteriorates as the imaging point moves farther away from the imaging center because of the aperture effect of the transducer, as described in the phantom results.[12]

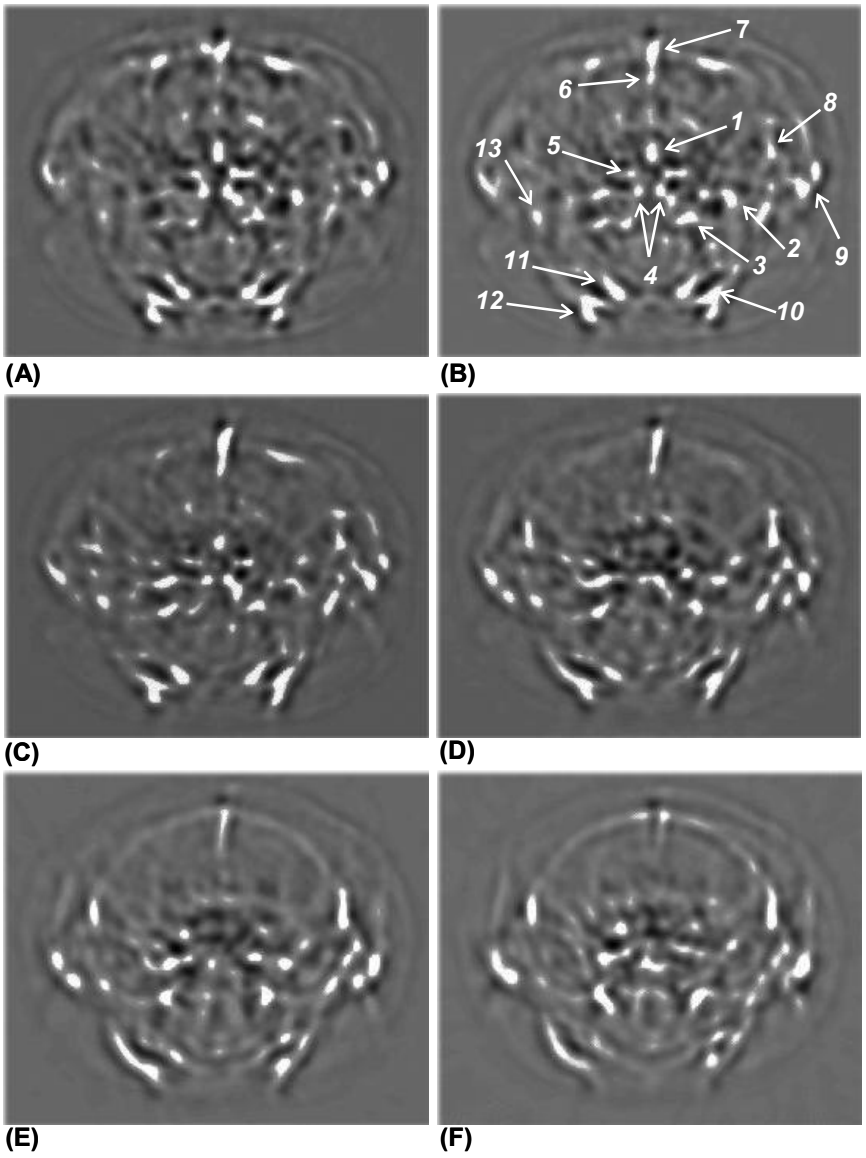

Figure 4. *In vivo* three-dimensional whole head images of the nude mouse from the coronal view, which were obtained from the anterior to the posterior parts of the brain every 1mm. Bright spots in the images represent sites of the high optical absorption, such as blood vessels.

4. DISCUSSION

A number of changes should be made to improve the image quality demonstrated here. First, the data acquisition time for a one slice image is currently 13 minutes. This amount time is much too long for studies involving certain physiological processes, such as dye circulation, which has a short clearance time through the head.

The acquisition time here is predominantly based on the circular scanning that used a single transducer. Therefore, we can increase the scanning speed by employing a transducer array, which will allow us to research the quick responses of the brain activity to extraneous stimuli.

Second, this imaging system has an uncontrolled slice thickness for several reasons: first, a flat transducer has a wide-signal-reception angle; second, the light illuminates objects broadly from the ground glass, and, third, the light is also scattered inside the various biological tissues. For a more precise quantitative study of biological parameters, better control of the slice thickness is necessary. Using a cylindrically focused transducer would improve the slice thickness.

Third, the resolution of the system was satisfactory to obtain the three-dimensional whole head images of the small animals; however, adjacent two blood vessels, like the facial artery and the jugular vein numbered 10 and 12 in the figure 3, respectively, were not clearly resolved due to the low resolution compared to the size of the blood vessels and the distance between them. When a high frequency transducer was employed to improve the resolution, the quality of the images became less to the contrary because of low sensitivity of the transducer. Employing a higher frequency transducer with higher sensitivity will improve the image quality as well as the resolution.

Lastly, we can improve the image quality by correcting for the speed aberration that is due to inhomogeneous tissues, such as the brain, muscle, and blood vessels. Our reconstruction algorithm-modified back projection assumes that the light energy and acoustic speed distributions are homogeneous through the imaging plane. However, these two assumptions are basically untrue because the light energy distribution is inhomogeneous because of the application of side illumination and the different optical absorption of various biological tissues; the acoustic speed distribution is also not homogenous because different tissues have different speeds of sound when ultrasound travels through them. Therefore, correcting the current algorithm in consideration of these two assumptions is necessary to improve the image quality.

5. CONCLUSION

In vivo three-dimensional whole head imaging by photoacoustic tomography was successfully accomplished. Related previous studies have been conducted, but they were limited to *in situ* imaging and could not clearly image deeply located arterial vessels. We imaged deep arterial vessels as well as superficial venous vessels with satisfactory resolution and contrast. One of the deep arterial vessels that we imaged, the arterial circle of Willis, provides oxygen to the brain. This can be a parameter used to monitor the brain activity response to extraneous stimuli. The simultaneous imaging of arterial and venous vessels will provide a basis for the functional imaging, such as oxygen consumption in the brain and cerebral blood volume (CBV). These are the most important parameters for studying brain tumors, ischemia, and strokes.[15]

ACKNOWLEDGEMENT

We thank Jung-Taek Oh, Meng-Lin Li, Konstantine Maslov, Geng. Ku and Xueyi Xie for fruitful laboratory assistance and Sergio Similache for assistance with animal handling. The project sponsored by National Institutes of Health grants R01 EB000712 and R01 NS46214. L. Wang's email is lwang@tamu.edu.

REFERENCE

1. S. L. Jacques, S. A. Prahl, Absorption spectra for biological tissues, http://omlc.ogi.edu/
2. R. O. Esenaliev, A. A. Karabutov, and A. A. Oraevsky, Sensitivity of Laser Opto-Acoustic Imaging in Detection of Small Deeply Embedded Tumors, IEEE J. S. T.Quantum Electron., Vol. 5, No. 4, 981-988 (1999)

3. X. Wang, Y. Xu, M. Xu, S. Yokoo, E. S. Fry and L.-H. V. Wang, Photoacoustic tomography of biological tissues with high cross-section resolution : Reconstruction and experiment, Med. Phys. 29, 2799-2805 (2002)
4. G. Ku, X. Wang, G. Stoica, and L.-H. V. Wang, Multiple-bandwidth photoacoustic tomography, Phys. Med. Biol. 49 1329-1338 (2004)
5. X. Wang, Y. Pang, G. Ku, X. Xie, G. Stoica, and L.-H. V. Wang, Noninvasive laser-induced photoacoustic tomography for structural and functional in vivo imaging of the brain, Nature Biotechnol. Vol. 21, No. 7, 803-806 (2003)
6. C. G. A. Hoelen, F. F. M. de Mul, R. Pongers, and A.Dekker, Three-dimensional photoacoustic imaging of blood vessels in tissue, Opt. Lett, Vol. 23, No. 8, 648-650 (1998)
7. X. Wang, G. Ku, M. A. Wegiel, D. J. Bornhop, G. Stoica, and L.-H. V. Wang, Noninvasive photoacoustic angiography of animal brains in vivo with near-infrared light and an optical contrast agent, Opt. Lett., Vol. 29, No. 7, 730-732 (2004)
8. X. Wang and L.-H. V. Wang, Three-dimensional laser-induced photoacoustic tomography of mouse brain with the skin and skull intact, Opt. Lett., Vol. 28, No. 19, 1739-1741 (2003)
9. R. A. Kruger, W. L. Kiser Jr, D. R. Reinecke, G. A. Kruger, and K. D. Miller, Thermoacoustic Optical Molecular Imaging of Small Animals, Molecular Imag. 2, Vol. 2, No. 2, 113-123 (2003)
10. American National Standards Institute, American national Standard for the Safe Use of Lasers ANSI Z136.1-2000 (American National Standards Institute, New York, 2000)
11. K. Maslov, G. Stoica, and L.-H. Wang, In vivo dark-field reflection-mode photoacoustic microscopy, Opt. Lett., Vol. 30, No. 6, 625–627 (2005)
12. M. Xu and L.-H. V. Wang, Analytic explanation of spatial resolution related to bandwidth and detector aperture size in thermoacoustic or photoacoustic reconstruction, Phys. Rev. E 67, 056605, (2003)
13. G. Ku and L.-H. Wang, Scanning microwave-induced thermoacoustic tomography: signal, resolution, and contrast, Med. Phys., Vol. 28, 4–10 (2001).
14. S. T. Flock, S. L. Jacques, B. C. Wilson, W. M. Star, M. J. C. van Gemert, Optical Properties of Intralipid: A phantom medium for light propagation studies, Lasers in Surg. Med. Vol. 12, No. 5, 510-519 (1992).
15. H. Elleaume, A.M. Charvet, S. Corde, F. Estève and JF Le Bas, Absolute Cerebral Blood Volume and Blood Flow Measurements Based on Synchrotron Radiation Quantitative Computed Tomography, J. of Cereb. Blood Flow Metab., Vol. 23, No. 4, 499−512 (2003)